

## **Robust Supramolecular Composite Hydrogels for Sustainable and “Visible” Agriculture Irrigation**

Chenfeng Ding<sup>1,2,4</sup> †, Shuai Zhang<sup>3</sup> †, Xuewei Fu<sup>2\*</sup>, Tuan Liu<sup>2</sup>, Lin Shao<sup>2</sup>, Mingen Fei<sup>2</sup>, Cheng Hao<sup>2</sup>, Yuan Liu<sup>1\*</sup>, Wei-Hong Zhong<sup>2\*</sup>

*1 State Key Laboratory of Bio-fibers and Eco-textiles, Institute of Biochemical Engineering, College of Materials Science and Engineering, Qingdao University, Qingdao 266071, China*

*2 School of Mechanical and Materials Engineering, Washington State University, Pullman, WA 99164, USA*

*3 School of Chemical and Biological Engineering, NingboTech University, Ningbo 315100, China*

*4 Foshan (South China) Institute for New Materials, Foshan 528200, China*

*† These authors contributed equally.*

**Supporting Information**

## **Experimental section**

### **Materials and chemicals**

Bacterial cellulose (BC) was supplied by Hainan Laize Biochemical Co., China. The polymerization degree of the bacterial cellulose was around 5000. Glycerol (>99%) and ethylene glycol diglycidyl ether (EGDE, epoxy value = 0.76 mol 100/g) were purchased from Tokyo Chemical Industry, Japan. Succinic anhydride (SA, 99%) was provided by ACROS Organic, China. Chloroform-d ( $\text{CDCl}_3$ , 99.8%) and dimethyl sulfoxide-d ( $\text{DMSO-d}_6$ , 99.9%) in this study were purchased from Sigma-Aldrich Co. Ltd., USA. The potassium hydroxide (>98%, KOH) was purchased from Beijing Tongguang Chemical Research Institute, China. All other chemical reagents were analytical grade and without further purification.

### **Preparation of bacterial cellulose skeleton**

The raw BC slices ( $5\text{ cm} \times 5\text{ cm} \times 0.5\text{ cm}$ ) were immersed in 1 M KOH solution at  $80\text{ }^\circ\text{C}$  for 8 h and then rinsed in deionized water to remove the KOH. The BC slices were physically crushed (12 000 rpm/min) in 100 mL of deionized water before adding 100 mL of acetone. The mixture was maintained for 24 h. Then the BC slices were collected, and then rinsed with ethanol alcohol and deionized water, respectively. Subsequently, the obtained dispersions with different concentration (7.5, 9.5, 11.5, 13 mg/mL) were transferred to desired molds, degassed in a vacuum oven for 4 h, frozen liquid nitrogen ( $-196\text{ }^\circ\text{C}$ ) and then freeze-dried at  $-50\text{ }^\circ\text{C}$ .

### **Synthesis of GSE precursor**

Glycerol (35 g), SA (38 g), and EGDE (100 g) were mixed and reacted under magnetic stirring at  $130\text{ }^\circ\text{C}$  for 1 h and  $150\text{ }^\circ\text{C}$  for 40 min, respectively. The corresponding molar ratio of glycerol monomer, SA monomer, and epoxy group of EGDE was fixed at 0.5:0.5:1 in this study.

### **Fabrication of double cross-linked supramolecular composite hydrogels**

The synthesized GSE precursor was gradually added to the surface of BC skeleton in the different molds. The mixture was degassed in a vacuum oven at room temperature for 1 h. The degassed samples were transferred to an oven at 150 °C for 3 h and then 190 °C for 3 h, respectively. The as-prepared composites were immersed in the deionized water for 10 h for absorption. As comparison, the synthesized GSE precursor was prepared by the same procedure which was denoted as GSE-HG.

### **Surface and structure characterization**

The weight of samples and chemicals were measured using an ultra-micro balance (Mettler Toledo) with an accuracy of 10 µg. Then the density (apparent density) of BC skeleton were measured according to the ISO standard 845:2006. The compression tests were conducted using a universal machine (Instron) with a 100-N load cell with a strain rate of 10 mm/min for  $\sigma$ - $\epsilon$  tests and 100 mm/min for cyclic fatigue tests. The microscopic architecture and chemical structure of samples were characterized by SEM (FE-SEM, Supra55, Carl Zeiss) and Fourier transform infrared spectroscopy (FT-IR) (Nicolet IS50). The molecular weight was measured using a gel permeation chromatography (GPC, Viscotek) system with a GPC max<sup>TM</sup> pump/autosampler/degasser module and a multi-detector (TDA 305). A HPLC grade tetrahydrofuran (THF) was used as eluent with a flow rate of 1.0 mL/min. Nuclear magnetic resonance (NMR) spectra were characterized using a Varian 400-NMR spectrometer (400 MHz) with CDCl<sub>3</sub> or DMSO-d<sub>6</sub> as the deuterated solvent. Chlorobenzene (20 mg) was added into 1 mL CDCl<sub>3</sub> as an internal standard.

### **In-situ characterization on curing process of GSE**

The curing process of synthesized GSE solution was characterized via a rheometer (TA Instruments, Discovery, HR-2) with parallel plates ( $D = 25$  mm). The samples were tested at  $150$  °C with a frequency of  $10$  rad/s and a constant strain of  $0.5\%$ . At the temperature sweep model, the heating temperature during measurement was ranged from  $100$  to  $200$  °C with  $3$  °C/min under the same condition. At the frequency sweep model, samples were scanned from  $0.1$  to  $500$  rad/s at  $190$  °C with a constant strain of  $0.5\%$ . For all rheological tests, the gap was  $1$  mm.

### **Characterization of thermal stability**

The thermal behaviors were measured using a differential scanning calorimeter (DSC, Mettler-Toledo) from  $-50$  to  $280$  °C at a heating rate of  $5$  °C/min under nitrogen atmosphere. Thermal stability was measured using a thermo-gravimetric analyzer (TGA/DSC, Mettler-Toledo). The samples ( $\sim 10$  mg) were measured from  $50$  to  $800$  °C at a heating rate of  $10$  °C/min under nitrogen atmosphere. Dynamic mechanical properties were tested using a dynamic mechanical analyzer (DMA, TA Instrument Q800) in single cantilever mode. The specimen with a dimension of ( $35$  mm  $\times$   $10$  mm  $\times$   $1$  mm) was scanned from  $-50$  to  $150$  °C at a heating rate of  $3$  °C/min. The oscillation amplitude was  $15$   $\mu$ m, and the frequency was  $1$  Hz. Tensile property was tested based on ASTM D638 using type V dog bone samples. The test was carried out on a universal test machine (Instron 4466) equipped with a  $10$  kN electronic load cell. The crosshead speed was  $1$  mm/min. The strain was monitored by clamping a one-inch extensometer (MTS 634.12E-24) on the test sample. For each formulation, at least five specimens were tested. The transparency was measured by UV-Vis transmission (JASCO V-670) in the region of visible light from  $360$  to  $760$  nm with a scanning rate of  $400$  nm/min. The dynamic water adsorption curves of samples were calculated by equation (1):

$$Q_{eq} = (m_2 - m_1)/m_1 \quad (1)$$

where  $m_1$  (g) and  $m_2$  (g) are the weights of the dry and swollen sample, respectively.  $Q_{eq}$  is calculated as grams of water per gram of sample.

Luminescence properties were carried out using a Cary Eclipse Fluorescence Spectrophotometer (Agilent Technologies). Samples were prepared into rectangular films (1 cm  $\times$  1 cm  $\times$  0.25 mm). The fluorescence spectra were scanned from 380 to 700 nm at an excitation wavelength of 365 nm with a selected slit width (Ex = 10, Em = 10). UV-Vis absorption spectra of samples were tested by a PerkinElmer spectrometer (Lambda 25). The samples were scanned from 200 to 600 nm. The photoluminescence quantum yield of the samples was measured in an integrating sphere by JASCO FP-8500 spectrophotometer. Time-resolved photoluminescence spectra of the samples were recorded by a time-resolved spectrometer (Hamamatsu, Streakscope). The photobleaching resistance test was carried by stimulated emission depletion nanoscopy (TCS SP8 STED3X, Leica) with 405 nm excitation beam.

Nitrogen adsorption/desorption isotherms were collected at 77 K on a Micromeritics ASAP 2020 instrument. The specific surface area was obtained by the Brunauer-Emmett-Teller (BET) method. The pore size distribution was obtained from density functional theory (DFT) method. The wetting behaviors were characterized by OCA 15 plus contact angle analyzer. The soil for evaluating the hydrogel stability was pre-treated in oven at 100 °C for 24 h.

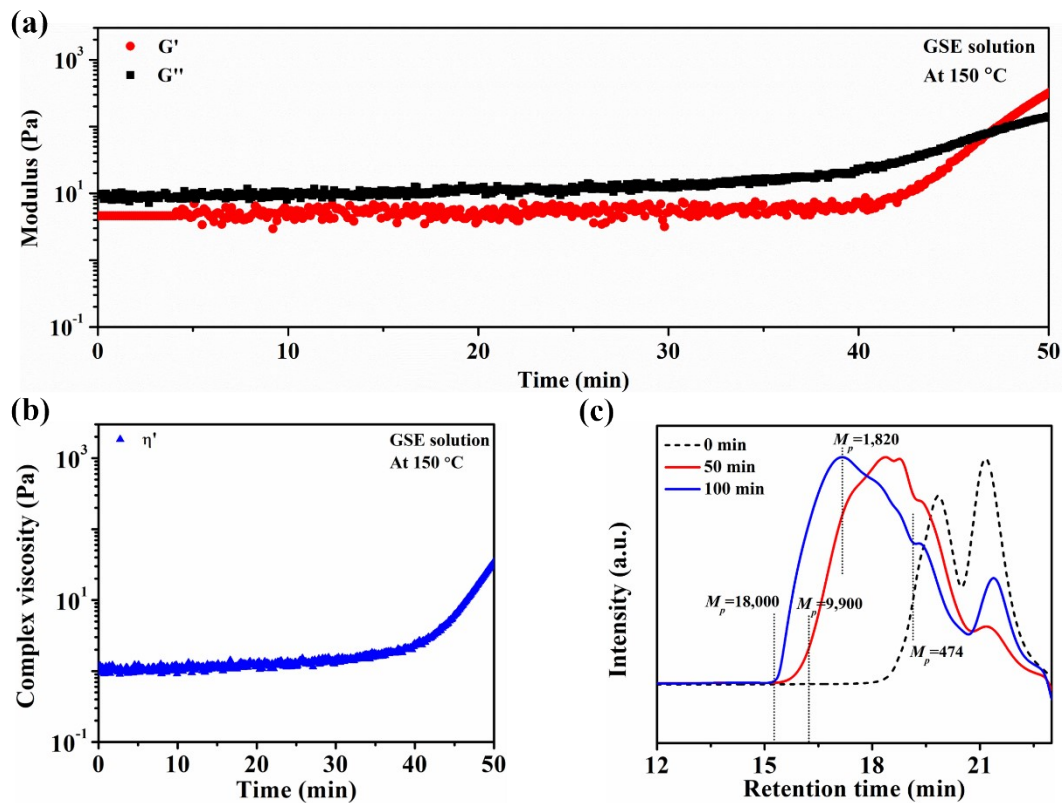


**Figure S1.** Changes of (a) storage modulus ( $G'$ ) and loss modulus ( $G''$ ), and (b) complex viscosity ( $\eta'$ ) of the GSE solution. (c) Gel permeation chromatography curves of GSE solution at different periods.

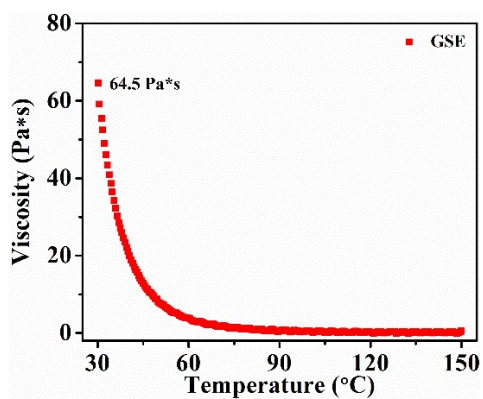


**Figure S2.** Viscosity of GSE prepolymer as a function of temperature.

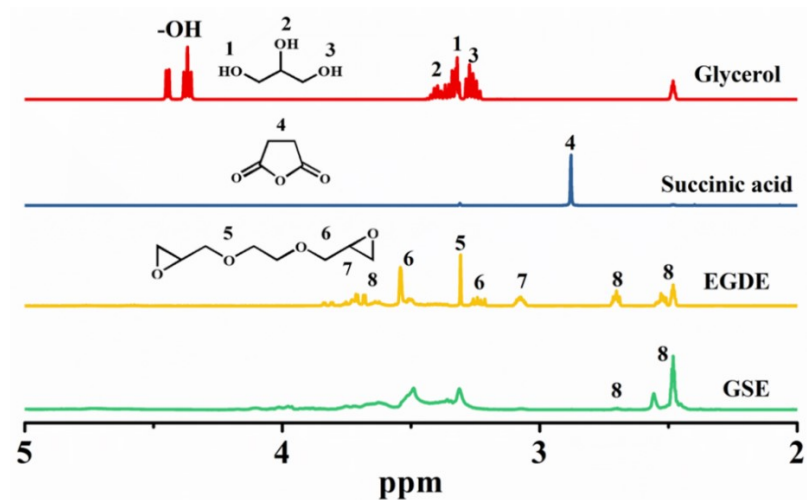


**Figure S3.**  $^1\text{H}$  nuclear magnetic resonance spectroscopy curves of GSE with counterparts.

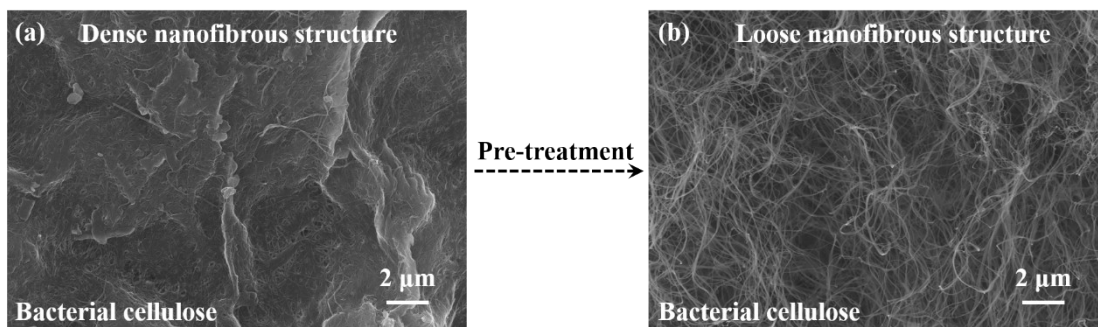


**Figure S4.** SEM images of nanofibrous structure of bacterial cellulose with (a) dense and (b) loose structure.

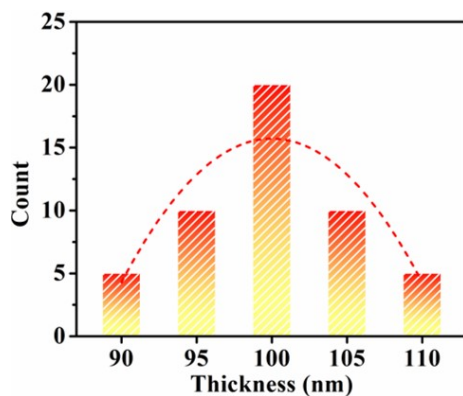


**Figure S5.** The thickness distribution of cell walls in BC aerogels.

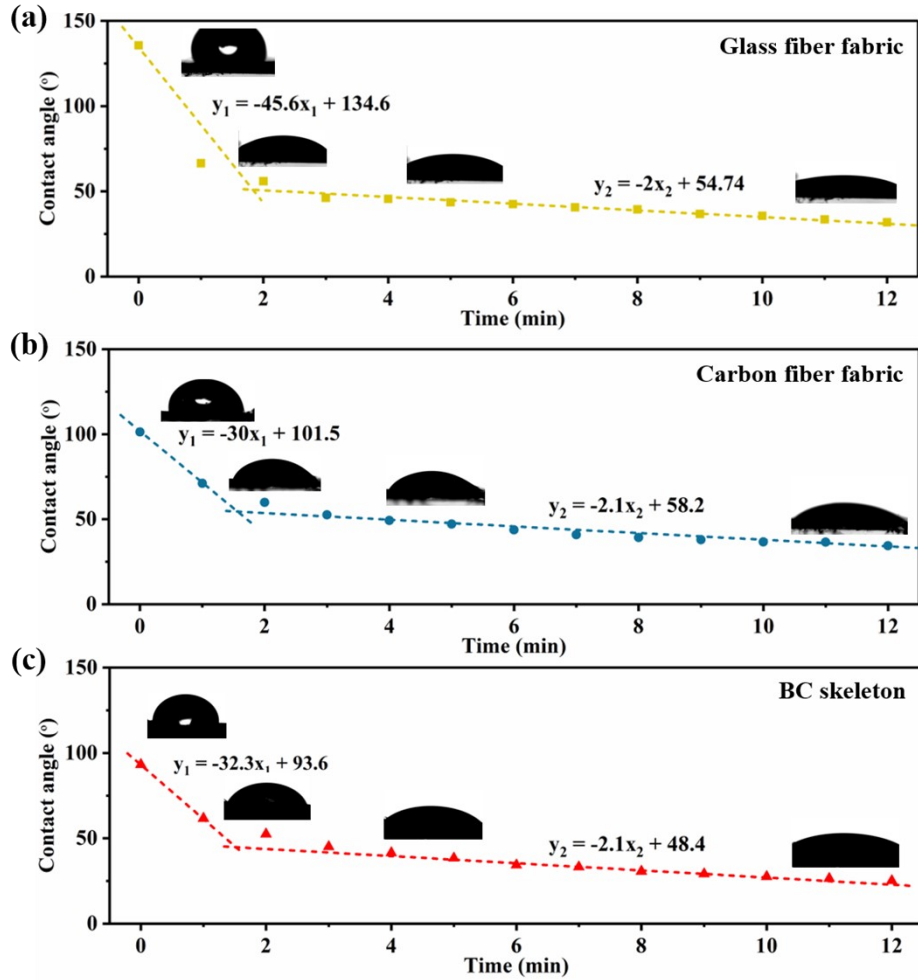


**Figure S6.** The infiltration process of GSE solution into BC porous matrix (c) as compared with glass fiber fabric (a) and carbon fiber fabric (b).

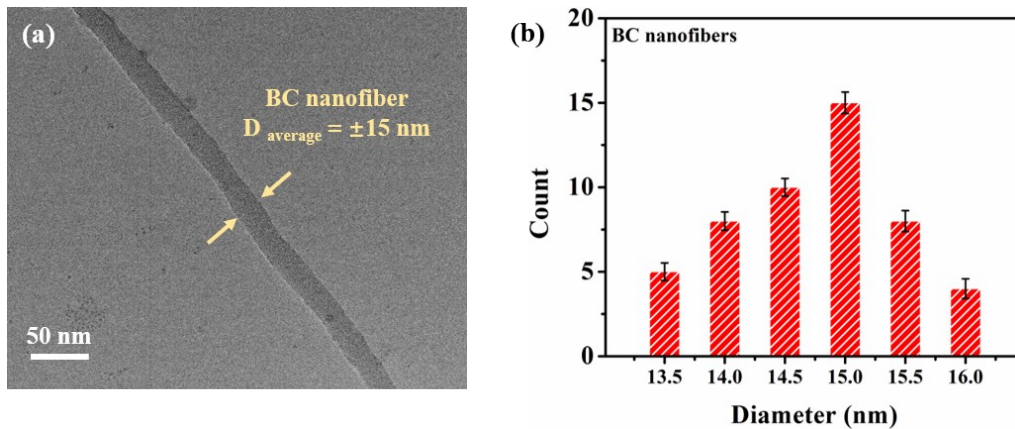


**Figure S7.** (a) High-resolution transmission electron microscopy image of BC nanofiber. (b) The diameter distribution of BC nanofibers in this study.

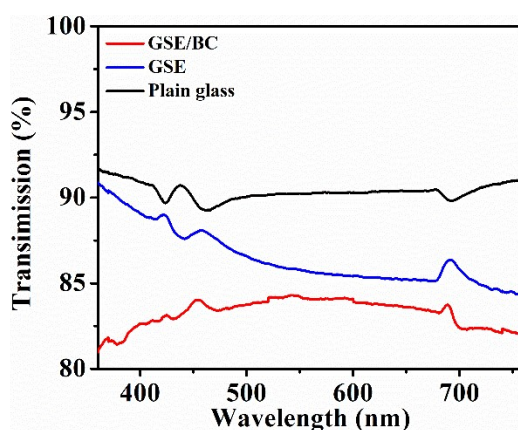


**Figure S8.** UV-Vis transmission spectra in the region of visible light from 360 to 760 nm of plain glass, GSE, and GSE/BC.

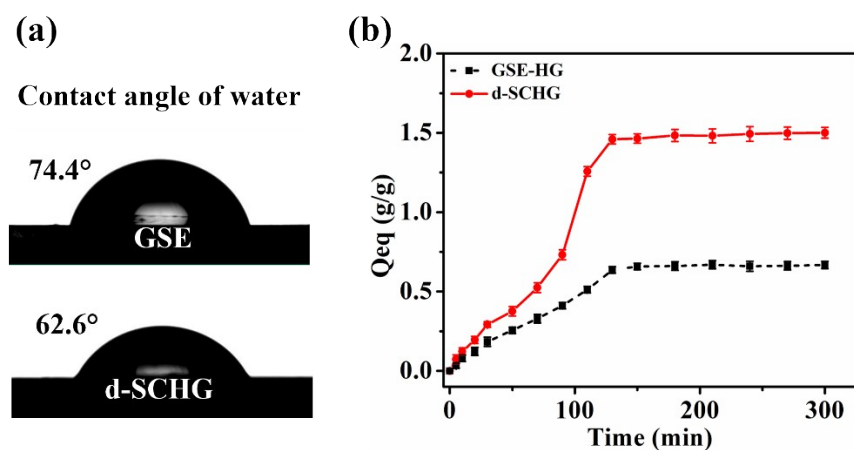


**Figure S9.** (a) The surface contact angle and (b) dynamic water adsorption curves of dry-state GSE and d-SCHG.

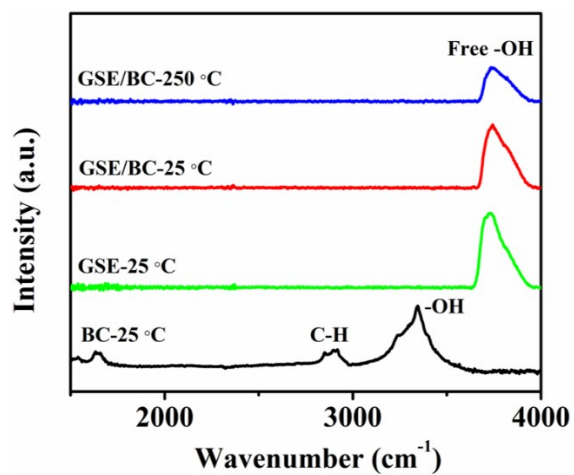


**Figure S10.** Fourier transform infrared spectroscopy curves of BC, GSE, GSE/BC at 25 °C and 250 °C for 1 h.

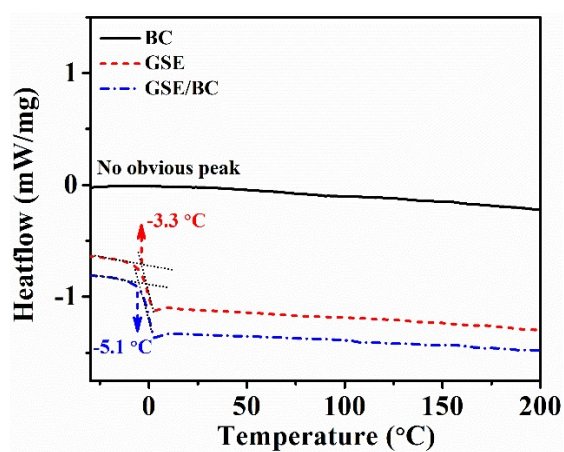


**Figure S11.** Differential scanning calorimetry curves of BC, GSE, GSE/BC.

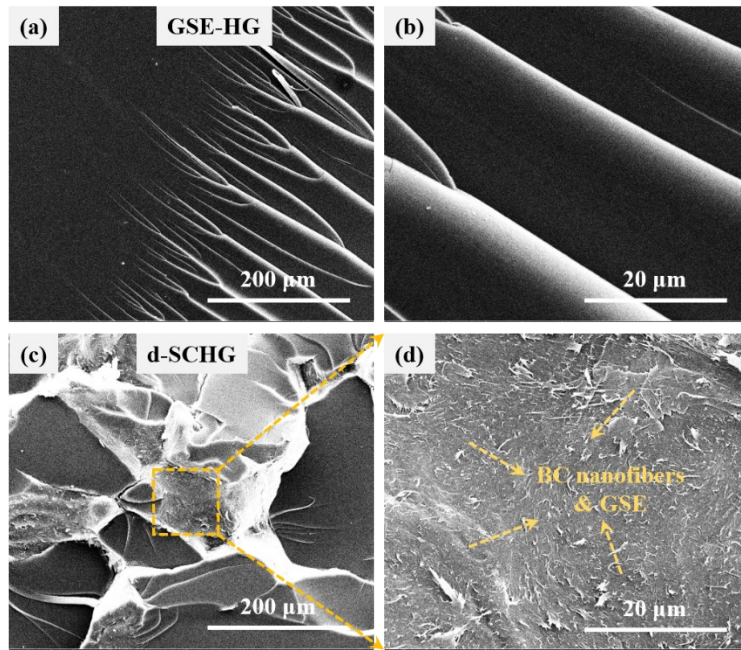


**Figure S12.** The sectional morphologies of (a, b) GSE-HG and (c, d) d-SCHG after tensile test.

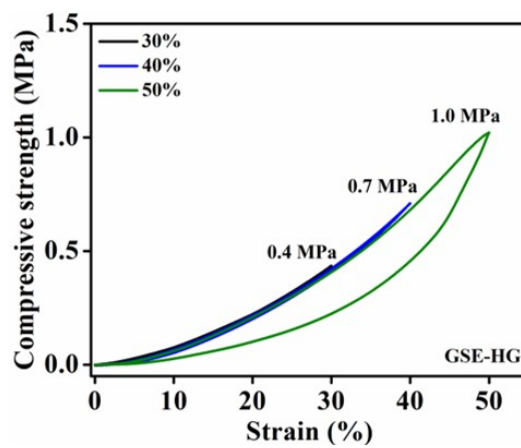


**Figure S13.** Compressive curves of GSE-HG with different strains (30%, 40%, and 50%).

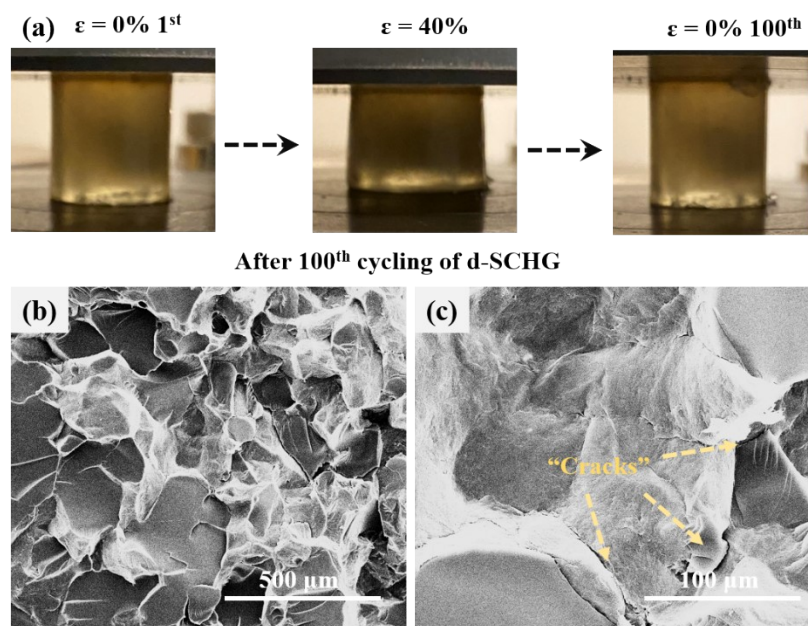


**Figure S14.** (a) Optical images of d-SCHG under various compressive strain and cycles. (b) and (c) SEM images of d-SCHG after 100<sup>th</sup> cycling.

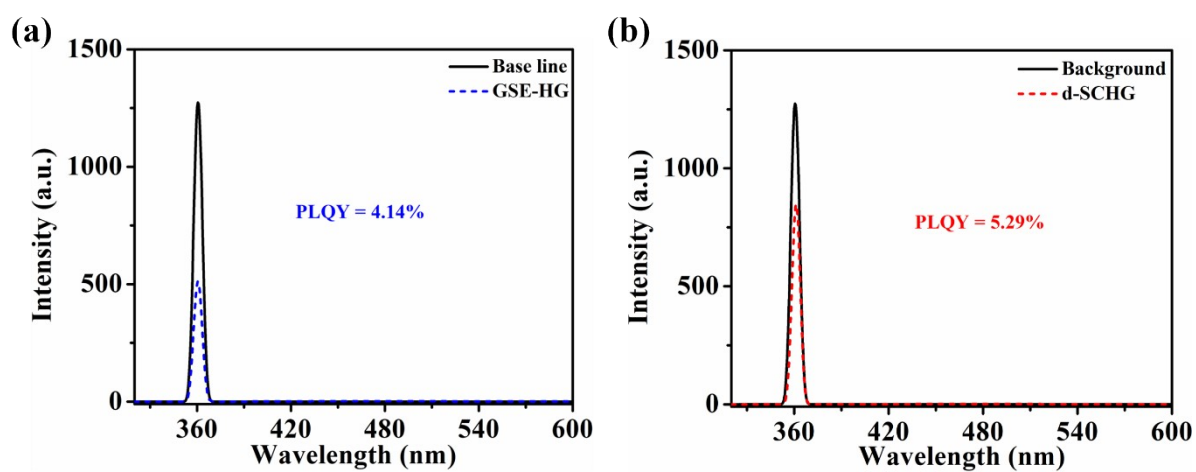


**Figure S15.** (a) Photoluminescence quantum yield (PLQY) of (a) GSE-HG and (b) d-SCHG at the wavelength of 360 nm.

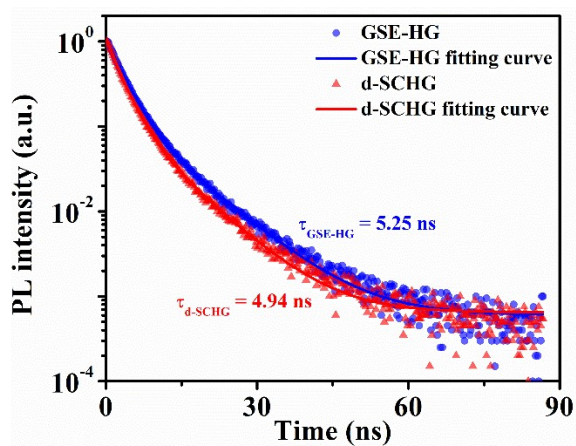


**Figure S16.** Photoluminescence lifetime of GSE-HG and d-SCHG at 405 nm.

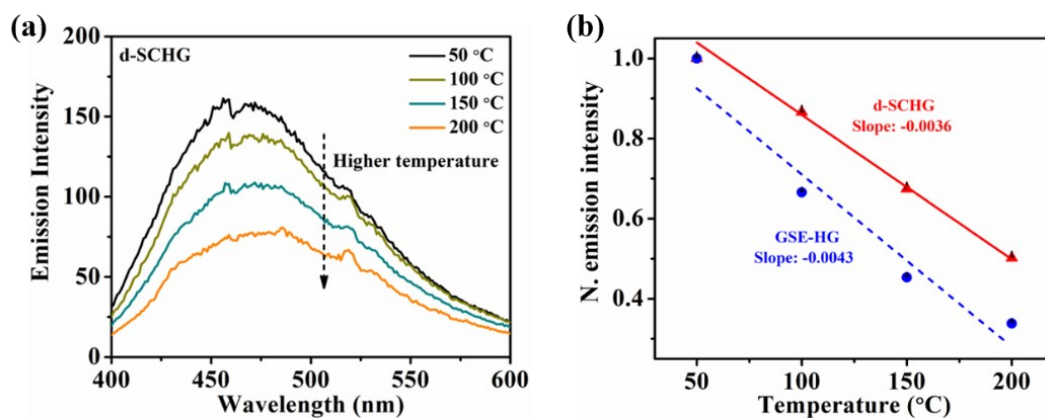


**Figure S17.** (a) Fluorescence spectra of d-SCHG at different temperatures. (b) Normalized emission intensity of d-SCHG and GSE-HG at various temperatures.

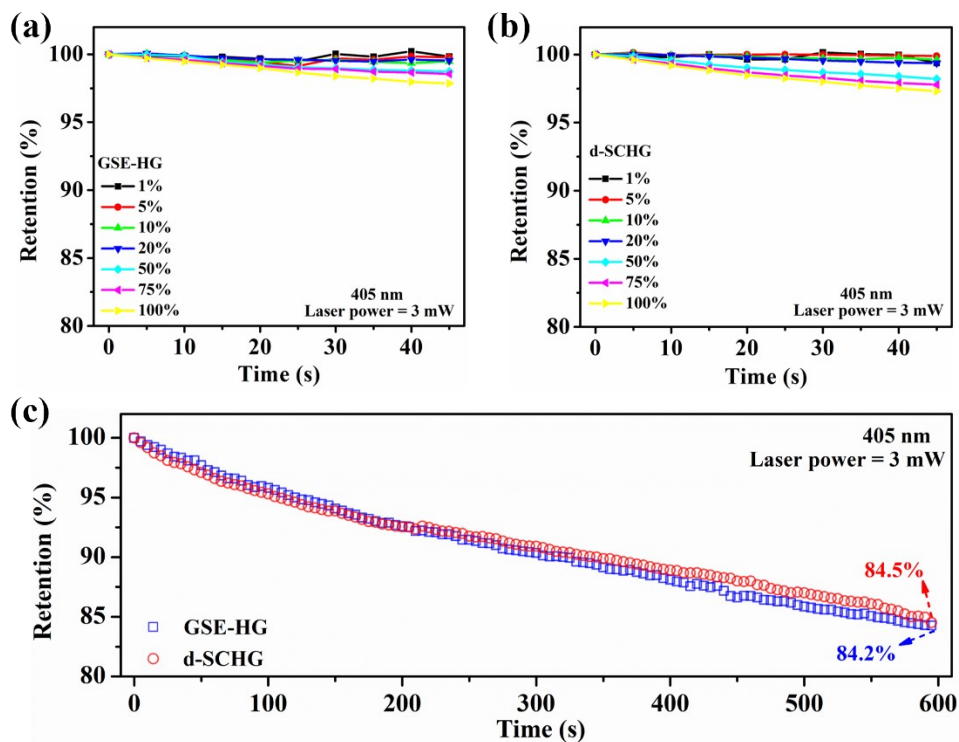


**Figure S18.** Normalized fluorescence intensity of (a) d-SCHG and (b) GSE-HG under various power of 405 nm excitation beam. (c) Normalized fluorescence intensity of d-SCHG and GSE-HG under 405 nm excitation beam with a power of 3 mW for 10 min.

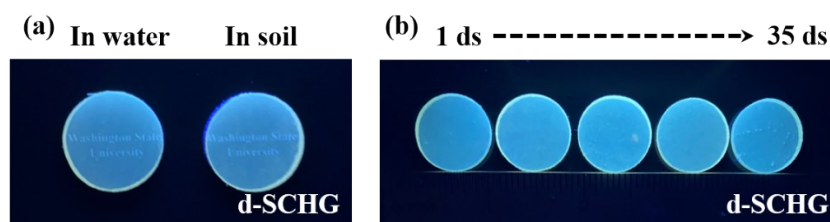


**Figure S19.** (a) Fluorescence spectra of d-SCHG at different temperatures. (b) Normalized emission intensity of d-SCHG and GSE-HG at various temperatures.

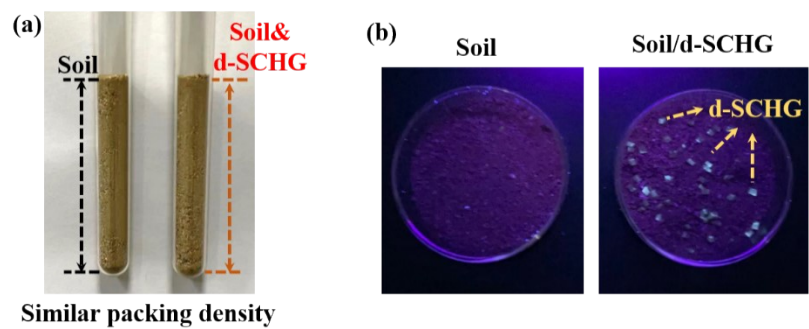


**Figure S20.** (a) Packing density and (b) optical images under the light with 365 nm of soil and that mixed with d-SCHG.